

Soft-x-ray amplification in a capillary discharge

Hyun-Joon Shin, Dong-Eon Kim, and Tong-Nyong Lee

Department of Physics, Pohang University of Science and Technology, Pohang 790-600, Korea

(Received 19 January 1994)

Soft-x-ray amplification in the C VI Balmer α transition is observed in a capillary discharge. The capillary is made of polyethylene with a bore diameter of 1.2 mm. A hot and dense carbon plasma which is formed on the capillary axis region expands radially and collides with the wall where it undergoes a rapid cooling and subsequent recombination. The amplification takes place in this cool ($T_e \sim 13$ eV) plasma region, according to space-resolved spectral data obtained using a 2-m grazing incidence spectrograph. The gain coefficient is measured to be 2.8 cm^{-1} .

PACS number(s): 52.80.-s, 42.55.Vc, 52.75.-d

I. INTRODUCTION

Since the early experiments based on the electron collisional [1] and the recombination [2] pumping schemes, great progress [3–9] has been made in understanding and improving the performance of soft-x-ray lasers in a large variety of lasing wavelengths [10]. In these existing schemes the pumping power is delivered onto a suitable target by focusing a high-power driving-laser beam. In addition to the high pumping power required [10] for short wavelength lasers, since the efficiencies of both the driver itself and the coupling between the driver laser light and the plasma are poor, the overall energy efficiency of the x-ray laser is extremely low. A practical soft-x-ray laser needs to be more energy efficient, compact, inexpensive, and easy to maintain. To this end, there have been a number of suggestions to utilize discharge plasmas as a lasing medium, including the capillary discharge.

Rocca, Beethe, and Marconi [11] have proposed the possibility of obtaining amplified spontaneous emission in a capillary discharge of a large (~ 100) aspect ratio (length to diameter ratio). Using a time-dependent collisional radiative model, they predicted a gain coefficient of 5 cm^{-1} for the C VI Balmer α (H_α) line (18.2 nm) radiation in a carbon plasma created by a 0.1 mm diameter, 20 mm long capillary discharge. The mechanism for the population inversion in the model is the recombination due to conductive cooling of the hot plasma to the capillary wall.

Recently, Steden and Kunze [12] reported the observation of an enhanced photoelectric signal [a few nanoseconds full width at half maximum (FWHM) duration] from the C VI H_α line emission in a polyacetal capillary discharge. They claimed a maximum gain coefficient of 3.1 cm^{-1} . However, there remains a few questions to be cleared before an unambiguous confirmation, including an improved gain coefficient measurement and an understanding of a gain pulse during the second half cycle of the discharge rather than the first half cycle. There have been so far unsuccessful attempts [13] by others to reproduce the experiment.

Electric breakdown in a capillary discharge may take

place initially along the inner wall, since this is the least inductive current path, as in many linear pinch devices [14]. The plasma current sheath which is formed by the ablated material from the surface breakdown will then implode radially toward the capillary axis. In order to heat the plasma to a high enough temperature to produce a large number of fully-stripped ion species, one would like to have a tight pinch (i.e., a large pinch ratio). However, such a pinched plasma fragments into a number of beadlike segments [15] which could decrease the uniformity of the plasma medium for amplification. Nevertheless, the plasma condition should be such that it can ionize the bulk of carbon atoms to C^{6+} ions within a short period of time. The plasma now expands radially from the stagnation and eventually collides with the capillary wall. There the plasma will experience a sudden cooling, mainly due to conduction loss to the wall, and subsequent recombination. If the plasma condition is right then the outer annulus region close to the wall is likely the place where the amplification will take place. It is therefore important to observe this region exclusively, because the mixing of the contribution from other regions may obscure the net effect of gain.

In the present study, we report unambiguous observation of an amplified spontaneous emission in the C VI H_α transition. The result is obtained from space-resolved and time-resolved spectral data, using a polyethylene capillary discharge. The gain in the C VI H_α transition is directly verified by comparing spectral line intensities of the gain and nongain lines by varying the capillary length.

II. EXPERIMENTAL ARRANGEMENT

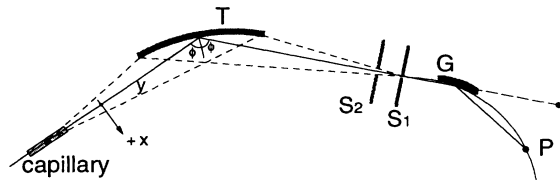
Throughout the experiment, polyethylene capillaries [16,17] with a 1.2 mm bore diameter were used, and their lengths were varied from 8 to 16 mm. The capillary discharge was powered by two low-inductance capacitors (60 nF each) connected in parallel to the capillary electrodes via identical transmission lines. The discharge was initiated by a carbon trigger-pin inserted near one of the electrodes. The charging voltage was varied from 17 to 27 kV; and the discharge current was monitored for every

discharge by a Rogowski coil. The half-cycle time of the discharge was typically 220 ns (145 ns FWHM for the 14 mm long capillary). The change in half cycle time of the discharge (due to inductance change) caused by the capillary length variation is within 10%, according to a number of measurements with capillaries of different length. Throughout the experiment, the input power density [= (stored energy)/(capillary volume)/(FWHM) of the discharge current] of the capillary volume is kept the same ($1.5 \times 10^{10} \text{ W cm}^{-3}$) by adjusting the capacitor charging voltage for different capillary lengths.

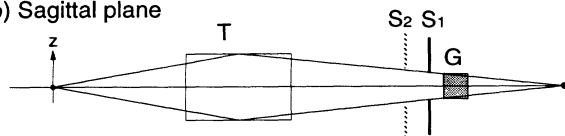
A toroidal mirror (with a minor radius of 4.5 cm and a variable major radius by bending) is placed between the capillary and a two-meter grazing-incidence spectrograph monochromator to collect light from the discharge into the spectrograph through the entrance slit, as can be seen in Fig. 1. Throughout the investigation, the distance from the center of the capillary length to the center of the toroidal mirror is taken as an object-to-mirror distance; and the incidence angle to the toroidal mirror in the meridional plane is kept around 85.7° [see Fig. 1(a)]. A ray tracing program is used in this investigation in order to determine the required parameters. A stigmatic spectral image can be formed by focusing at a desired wavelength region on the Rowland circle in the sagittal plane [see Fig. 1(b)]. A spherical grating of 600 lines/mm which is set at a grazing angle of 1.5° is used with a $22\text{-}\mu\text{m}$ -wide entrance slit. The reciprocal dispersion of the spectrograph at wavelengths of 4 and 18 nm are 0.62 and 1.2 \AA mm^{-1} , respectively.

Time-integrated spectra from the discharge were recorded on photographic plates (Kodak 101-05) and each plate was developed under identical conditions throughout the experiment. The optical density on each

(a) Meridional plane



(b) Sagittal plane



T : toroidal mirror S1 : entrance slit ($22 \mu\text{m} \times 9 \text{ mm}$)
 G : grating S2 : auxiliary slit ($2 \text{ mm} \times 14 \text{ mm}$)
 $\phi \sim 85.7 \text{ degree}$ Sagittal focus at $\lambda = 28.7 \text{ nm}$

FIG. 1. Schematic diagram showing the arrangement of the capillary light source, the toroidal mirror, and the grazing-incidence spectrograph: (a) view on the meridional (x, y) plane and (b) view on the sagittal (y, z) plane. Here, y axis indicates the optical axis defined by the spectrograph and the toroidal mirror system.

developed plate was compared against a calibrated diffuse density wedge, and the relative spectral intensities were then obtained using Henke's formula [18].

The alignment of the experimental setup was critical, i.e., a slight misalignment resulted in a large reduction in spectral intensity. The alignment is performed in two steps. First, a He-Ne laser was used as a backlighting source for the spectrograph, and the laser beam was set in such a way that it passed through the central image point, the center of the grating, and the entrance slit. The toroidal mirror and the capillary were then aligned with respect to the reference beam. A second He-Ne laser was placed one meter from the other end of the capillary and the laser beam from this end was made to coincide with (and be parallel to) the first reference beam. This second laser beam also served to check for misalignment due to vibrations during the evacuation of the mirror chamber.

III. RESULTS

A. Spatially resolved spectra

A toroidal mirror-spectrograph system, such as the present experimental setup, can give stigmatic focusing of a light source at the diffracted image of the spectrograph [see Fig. 1(b)]. This may give spatial resolution [19] in a direction perpendicular to the dispersion at a desired wavelength region, if the light source is small and the magnification of the system is reasonably large. Figure 2 illustrates microdensitometer scans of the C VI H_α line and the continuum nearby where stigmatic focus is made to occur. The scans are made in a direction perpendicular to the spectral dispersion. It is apparent that a stronger continuum is emitted at the axial region of the capillary, suggesting a dense and hot plasma on axis due

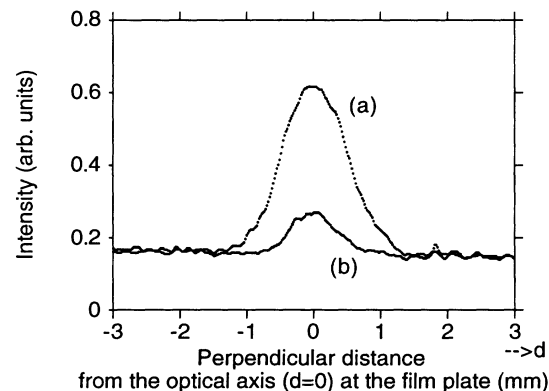


FIG. 2. Microdensitometer traces of the C VI H_α line (a) and nearby continuum (b) scanned in a direction perpendicular to the dispersion. The sagittal focus is made at the C VI H_α ($\lambda = 18.2 \text{ nm}$) and the optical axis is in coincidence with the capillary axis. In this case, the capillary diameter and the length are 1.0 and 14 mm, respectively. It can be seen that the continuum is mainly concentrated near the axial region whereas the H_α line radiation is emitted from more broader region of the capillary cross section.

to a radial pinch, as described above.

The toroidal mirror forms an astigmatic image of the light source at the entrance slit which is due to focusing in the meridional plane [see Fig. 1(a)]. The shape of the image at the slit is investigated using the ray tracing method. It is assumed that the light source is a 10 mm long cylinder where 600 seed rays with a uniform radial distribution originate. This is superposed by the concentrated seed rays of a 200- μm diam Gaussian distribution at the central region of the orifice. The divergence angle of the source rays are essentially determined by the acceptance angle of the toroidal mirror and the spectrograph, and are ± 15 mrad in the meridional plane and ± 20 mrad in the sagittal plane. A light source with a circular cross section becomes a banana-shaped astigmatic image with an elongated and curved central (dense) region at the slit. Let the y axis be the line of sight (optical axis) which is determined by the center of toroidal mirror and the spectrograph, and the perpendicular axis which lies in the meridional plane be the x axis [see Fig. 1(a)]. Three cases are considered, i.e., the case where (a), the y axis coincides with the axis of the capillary light source, (b) the capillary axis is moved 0.4 mm along the $-x$ -axis direction (toward the back side of the mirror) from the location (a), and case (c) where, the capillary axis is moved 0.4 mm in the $+x$ -axis direction from the location (a), keeping the capillary axis parallel to the y axis in all cases. The resulting ray-traced images formed at the entrance slit are shown in Fig. 3(A)(a), 3(A)(b), and 3(A)(c). In these cases, a different portion of the source radiation will be admitted to the spectrograph through the slit (22 μm in width and 9 mm in length), depending on the position of the slit relative to the image. Now suppose the stigmatic focusing at the photographic plate is made to occur at a much longer wavelength (29 nm) than those of the C VI H_α and other spectral lines under interest. Then the spectral image at the photographic plate on the Rowland circle will be different, depending on the slit position relative to the image. For instance, in the case of Fig. 3(A)(b), the slit intersects with the central region (a dense region) of the banana-shaped image at two locations; and the spectral image of the strong continuum from the axial region will look like a pair (representing two intersections of the dense curved region) of slowly converging narrow bands toward the 29 nm region. On the other hand, radiation which is coming from somewhere other than the axial region (i.e., the peripheral region) will be recorded between the two narrow (continuum) bands.

Time integrated spectra from the capillary discharge are obtained with the arrangement shown in Fig. 3(A)(a), 3(A)(b), and 3(A)(c). Microdensitometer scans of the continua (at 10 nm region) in a direction perpendicular to the dispersion are shown in Fig. 3(B)(a), 3(B)(b), and 3(B)(c), respectively. For Fig. 3(B)(b), the scan shows two humps which represent the continuum from the axial region. Radiation from the peripheral plasma is recorded by the region between the two humps. In the cases of (a) and (c), the scans show a broad single hump which represents the axial and peripheral region, respectively. The ray tracing confirms similar images at the photographic plate. It is therefore possible to obtain a space-resolved spectra [20]

by scanning a desired portion of the photographic plate using a microdensitometer. The spatial resolution that one can obtain using this technique depends on the wavelength. In this experiment, it is limited to 150–200 μm .

Figure 4(a) and 4(b) illustrate microdensitometer scans (in wavelengths of 2.5 to 4.2 nm) of a single-shot spectra which are obtained with the image position of Fig. 3(A)(a) and 3(A)(c), respectively. Figure 4(c) shows a microdensitometer scan of the same spectral plate as 4(b) but showing wavelengths of 2.5–20 nm which includes the C VI H_α line. The scans in Fig. 4(a), 4(b), and 4(c) are made at the peak of their hump and therefore represent the radiation from the axial (a) and the peripheral (b) and (c) regions of the capillary cross section. In the case of Fig. 4(a), there are strong Lyman series lines of H-like C VI and $n \rightarrow 1$ resonance lines of He-like C^{4+} ions. There is a relatively strong continuum on the short wavelength side of the C V series limit. However, one notices

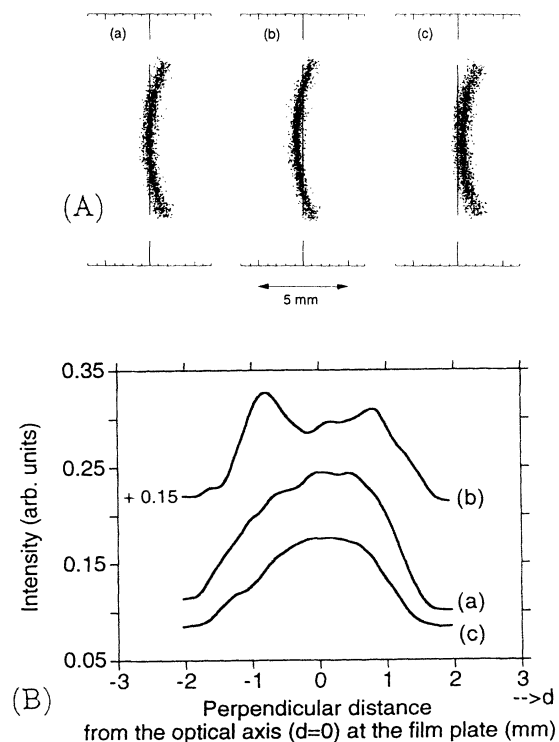


FIG. 3. (A): ray-traced (astigmatic) image of the capillary light source at the entrance slit (shown as a vertical line) of the spectrograph, showing three different locations of the capillary axis relative to the slit, i.e., the capillary axis (a) in coincidence with the optical axis or at $x = 0$, (b) at $x = -0.4$ mm, and (c) at $x = +0.4$ mm. Here, the capillary axis is always parallel to the y axis. The light source is assumed to be a 10 mm long cylinder where 600 seed rays with a uniform distribution originate. This is superposed by the concentrated seed rays of 200 μm Gaussian distribution at the central region of the orifice. (B)(a), (B)(b), and (B)(c): microdensitometer traces of experimental spectra obtained with the arrangement shown in (A)(a), (A)(b), and (A)(c), respectively, showing continuum at $\lambda = 10$ nm region scanned in a direction perpendicular to the spectral dispersion. In this case, the stigmatic focusing (in the sagittal plane) is made to occur at wavelength of 29 nm.

that the recombination continuum of C^{6+} ions beyond the Lyman series limit is very weak. The radiation from the peripheral region gives much weaker spectral features than that from the hot plasma region as can be seen in Fig. 4(b). However, the intensity of the C VI H_α line at 18.2 nm is still intense, as one sees in Fig. 4(c).

Time-integrated electron temperatures for both cases may be estimated from the slope of the recombination continuum of the C^{5+} ions. The continuum intensity may be expressed [21] as $I \sim \lambda^{-2} \exp(-hc/\lambda kT_e)$ and therefore a plot of $\ln(I\lambda^2) \sim hc/kT_e$ as a function of $1/\lambda$ (wave number) is a straight line. Figure 5 shows such plots for the plasma radiation which comes from the axial and the peripheral regions of the capillary. The obtained electron temperature of 25 eV at the axial region for the C^{5+} plasma may be somewhat lower than expected, possibly because this is the time-integrated temperature, not the peak temperature. However, even the peak temperature may not be very high, judging from the very weak

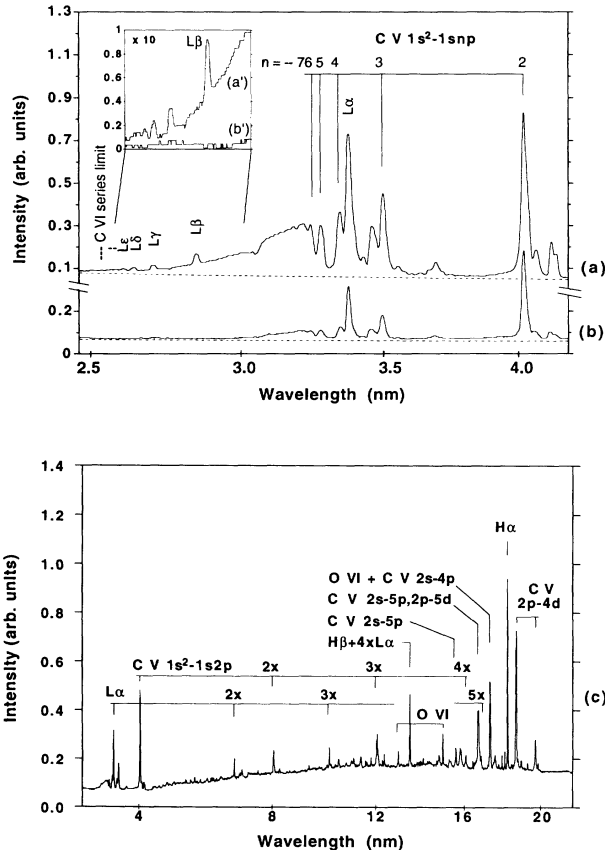


FIG. 4. Microdensitometer traces of time-integrated spectra in the wavelengths of 2.5–4.2 nm, representing plasma radiation from the axial (a) and from the peripheral (b) region of the capillary. Dotted lines in (a) and (b) indicate chemical fog level. The intensity dip which appears in the recombination continuum in (a) is due to an absorption line, possibly $NI K\alpha$, as an impurity. The inset, (a') and (b'), shows magnified ($\times 10$) version of a part of the continua in (a) and (b). (c) indicates a broadband spectral scan of the same spectral plate as (b), showing wavelength region from 2.5 to 20 nm.

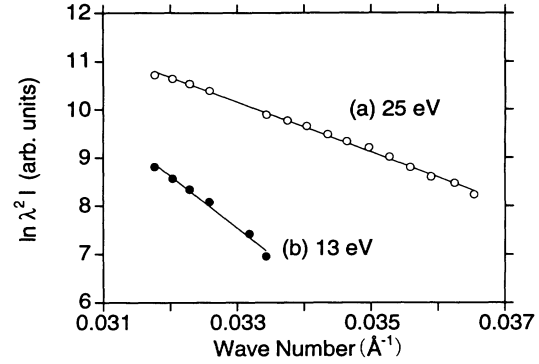


FIG. 5. Time-integrated electron temperatures determined from the slope of recombination continuum of the C^{5+} ion, at axial (a) and the peripheral (b) region of the capillary.

C VII recombination continuum described above. On the other hand, case (b), which represents the radiation exclusively from a part of the outer annulus region, indicates that the electron temperature there is 13 eV. According to the time-resolved spectroscopic observations described in III C, the intensity peaks of the C VI L_α , H_α lines and the continuum all occur at about 35–40 nsec after the discharge-current maximum. Therefore, a large contribution to the exposure of time integrated spectra is likely to be made mainly during this period. The timing of the electron temperature measurements may then coincide with the approximate time that the C VI H_α intensity peaks.

The branching ratios of $I(H_\alpha)$ ($n=3 \rightarrow 2$) to $I(L_\beta)$ ($n=3 \rightarrow 1$) for hot and cool regions may be obtained using spectra such as shown in Fig. 4 by comparing the line intensities. The L_β line intensity of the cool region $I(L_\beta)_{\text{cool}}$ is very weak compared with the $I(L_\beta)_{\text{hot}}$, as can be seen in the inset of Fig. 4(a') and 4(b'), i.e., $I(L_\beta)_{\text{hot}}/I(L_\beta)_{\text{cool}} > 15$. In the 18.2 nm wavelength region, the H_α intensity ratio for hot and cold plasma, $I(H_\alpha)_{\text{hot}}/I(H_\alpha)_{\text{cool}} \sim 1.5$ (not shown in Fig. 4); and, therefore, the branching ratios for hot and cool region of the capillary plasmas are $[I(H_\alpha)/I(L_\beta)]_{\text{hot}} \ll [I(H_\alpha)/I(L_\beta)]_{\text{cool}}$. This may be taken as evidence that there exists a population inversion between $n=3$ and 2 of the C^{5+} ions in the cool plasma region.

B. Gain measurement

In order to verify the gain in the cooler plasma, spectral radiation which originates mainly in the peripheral region is observed using the arrangement described above. The relative intensities of C VI H_α and other spectral lines nearby are measured by varying the capillary length. In this series of experiment special care is paid to exclude impurities in the discharge as much as possible and the input power density ($1.5 \times 10^{10} \text{ W/cm}^3$) was kept the same for all capillary lengths. Figure 6 shows the microdensitometer scans of time-integrated spectra for wavelengths of 10–23 nm, which are obtained with two different capillary lengths, 14 and 10 mm. Each spec-

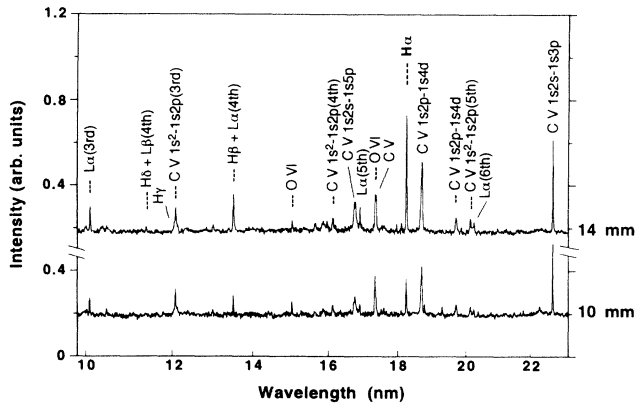


FIG. 6. Comparison of two time-integrated spectra obtained using capillary length of 14 and 10 mm, showing the C VI H_{α} and other lines in the 10 to 23 nm region. Each spectrum is obtained with a single discharge and with the input power density of $1.5 \times 10^{10} \text{ W cm}^{-3}$.

trum is obtained with a single-shot exposure, right after two low-voltage ($\sim 10 \text{ kV}$) cleaning shots with a newly prepared capillary.

The intense line radiation at 18.2 nm is the Balmer H_{α} line of the C^{5+} ion. Unfortunately, other members of the Balmer series lines are blended with either the high order lines of the Lyman series lines or the third order line of the CV resonance line. There are others which include the CV lines of $1s2s-1snp$, $1s2p-1snd$ transitions, and some impurity O VI lines in the spectra. The spectra shown in Fig. 6 indicate that the C VI H_{α} line intensity increases more rapidly than any other lines when the capillary length increased from 10 to 14 mm. In order to check the tendency, intensities of the major spectral lines in this wavelength region are plotted as a function of capillary length and these are shown in Fig. 7(a) and 7(b). The line intensities of the C VI L_{α} (third and fifth order), the C V $1s2p-1s4d$, and the $1s2s-1s5p$ transitions increase linearly, whereas the C VI H_{α} line increases exponentially with increasing capillary length, as can be seen in Fig. 7. The dotted line in Fig. 7(b) represents a gain curve with a gain coefficient of $g = 2.8 \text{ cm}^{-1}$, obtained from the formula given by Linford *et al.* [22]. Also plotted is the intensity of the C VI $H_{\beta}-L_{\alpha}$ (fourth order) blended line, indicating some evidence of gain for the C VI H_{β} transition. The C VI H_{α} line intensity for a 16 mm long capillary does not show exponential increase, but tends to level off, and this gives the gain-length product, gL value of 3.9 in the present experiment. This is a typical tendency in a recombination-pumped soft-x-ray amplifier where the gL values are much smaller [3] (typically, $gL \leq 4$) than those in the electron-collisionally pumped scheme [4–8]. It is also found that the gain in the C VI H_{α} transition is likely to be observed in the first few discharges using a newly prepared polyethylene capillary.

In a relatively large-diameter plasma which is produced in the present capillary (aspect ratio of 11.7) discharge, the reabsorption of the C VI L_{α} transition could be a serious problem for obtaining an amplification since it impedes prompt depletion of the lower gain level.

Considerable reduction in reabsorption at the line center may be achieved if the amplification takes place in a thin plasma layer in the vicinity of the capillary wall or/and when the radially expanding plasma (at a thermal velocity) collides with the wall (radial velocity zero), thereby creating a steep velocity gradient [10].

C. Time-resolved photoelectric signals

The temporal behavior of the spectral radiation is investigated by operating the spectrograph in a monochromator mode. A thin ($100 \mu\text{m}$) plastic scintillator was placed behind the $39\text{-}\mu\text{m}$ -wide exit slit and this was coupled to a photomultiplier tube (Hamamatsu H3284) outside the vacuum chamber via fiber optics cable. Figure 8(a), 8(b), and 8(c), show oscillograms of the discharge-current wave form and the photoelectric signals of the C VI H_{α} and the C V $1s2p-1s4d$ line, superposed with those of continuum in the vicinity of each spectral line.

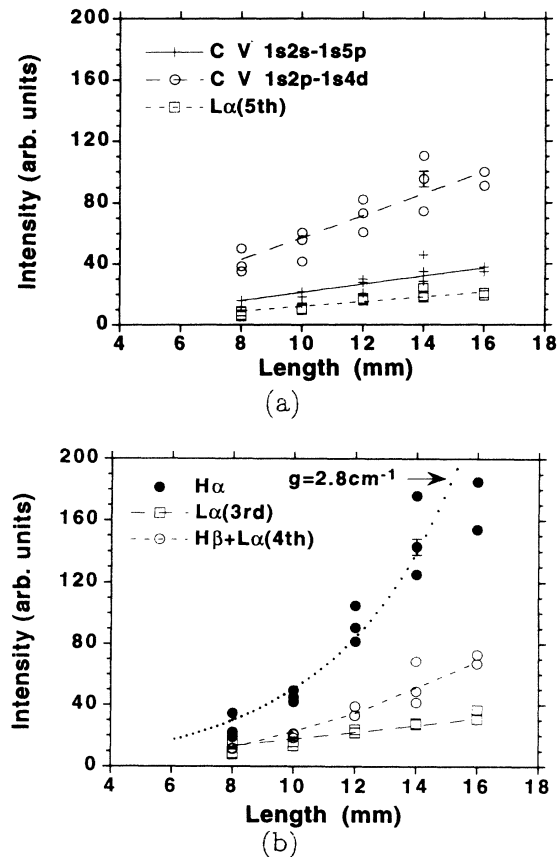


FIG. 7. Relative intensities of the C V $1s2s-1s5p$, $1s2p-1s4d$, and the C VI L_{α} (fifth order) lines as a function of capillary length (a). Relative intensities of the C VI H_{α} , the $H_{\beta}-L_{\alpha}$ (fourth order) blend, and the L_{α} (third order) lines vs capillary length (b). Each data point is obtained using a newly prepared capillary and with the same input power density of $1.5 \times 10^{10} \text{ W cm}^{-3}$. Typical error bars are indicated. The dotted line in (b) indicates the calculated gain curve with $g = 2.8 \text{ cm}^{-1}$. An attempt to make a straight-line fit of the H_{α} data points, instead of an exponential fit, would find that the straight line passes through point ($\sim 7 \text{ mm}$, 0) but not the (0,0) origin.

The time resolution of the photoelectric signal may be limited by the rise (a few nanoseconds) and the decay time [23] (< 2.2 ns) of the scintillator (NE 102) used in this experiment. The C VI H_α line signal peaks when the discharge current starts to decline from its first maximum. It has a pulse width of 60 ns FWHM. The CV line signal peaks much later (~ 40 ns) than that of C VI H_α signal, indicating a recombination of the C^{5+} ions.

Shot-to-shot intensity variation of the C VI H_α and the $1s2p-1s4d$ lines are examined from the spectral signals observed. Figure 9(a), 9(b), and 9(c) illustrate the line intensities of the C VI H_α and the CV $1s2p-1s4d$ for the different capillary lengths of 14 and 10 mm, as a function of the number of shots starting from the very first discharge (after two cleaning shots) using a same capillary. In the case of the 14 mm long capillary, the C VI H_α line intensity decreases very rapidly during the first four shots, whereas nongain lines do not change appreciably. In the case (b) of the shorter (10 mm) capillary, however, there is no such rapid decrease in signal height for either the C VI H_α or the CV line signals with an increase of number of shots. Also, it is found that an increase of the discharge power density to the 10 mm capillary neither enhances the intensity appreciably from the normal power density operation nor does it cause a rapid de-

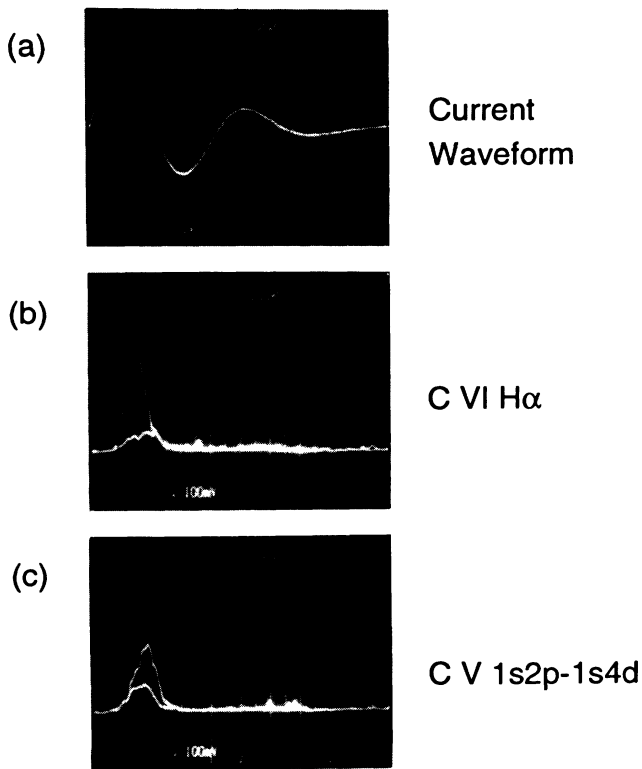


FIG. 8. Oscillograms of the discharge current wave form (a), the photoelectric signals of the amplified C VI H_α line (b), and the CV $1s2p-1s4d$ line ($\lambda = 18.67$ nm) (c). In (b) and (c), continuum signals near the respective line are superposed. In all cases, 14 mm long capillaries are used. Time scale is 100 nsec/div.

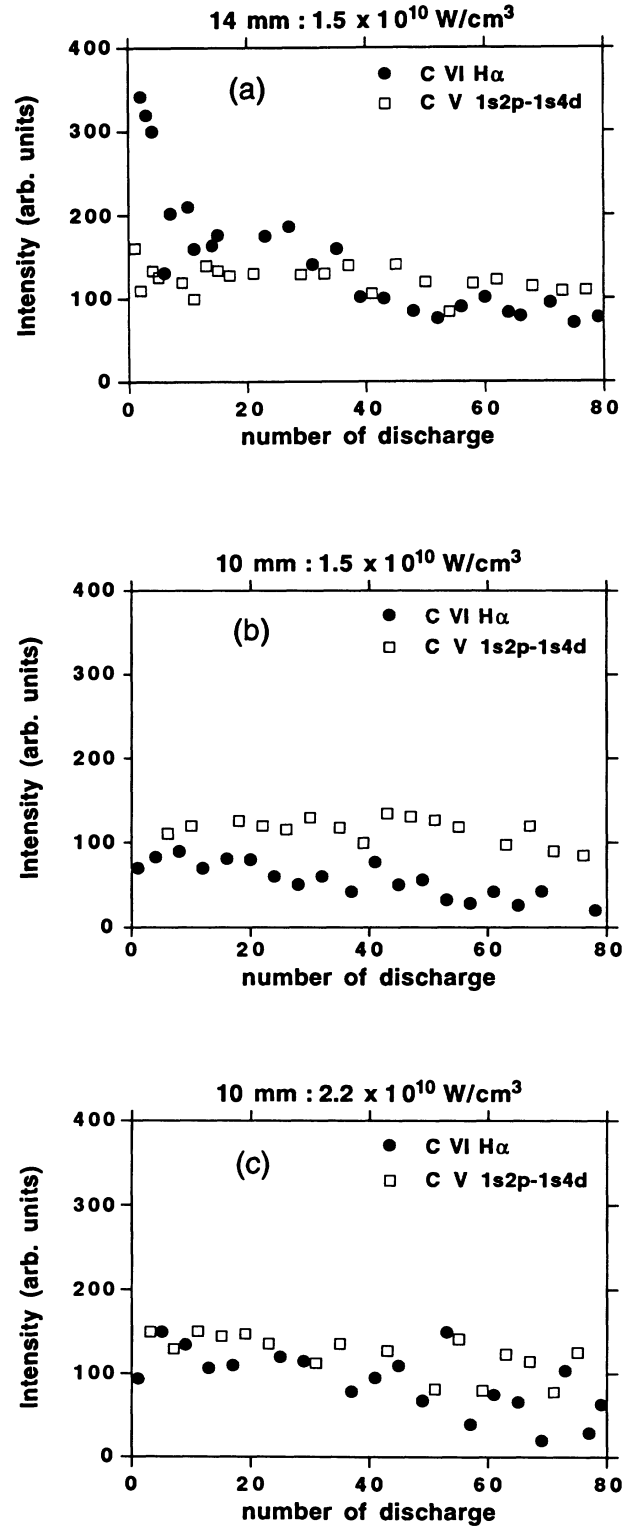


FIG. 9. Shot-to-shot variation of the C VI H_α and CV $1s2p-1s4d$ ($\lambda = 18.67$ nm) line intensities obtained from the respective photoelectric signals, starting from the very first (high energy) shot using the same capillary. In the cases of (a) and (b), 14 and 10 mm long capillaries are used at the same input power density of $1.5 \times 10^{10} \text{ W cm}^{-3}$, whereas in (c), a 10 mm long capillary at input power density of $2.2 \times 10^{10} \text{ W cm}^{-3}$ is used.

crease of intensity during the first few shots, as can be seen in Fig. 9(c). An examination of the capillary bore diameter after five shots indicates neither noticeable damage to the wall nor appreciable increase in diameter (corresponding to about 10% increase in volume in 14 mm capillary). These results based on the photoelectric signals are in good agreement with those obtained from the time-integrated spectra described above, i.e., (1) the gain exists only for the first few shots in a newly prepared capillary, (2) an increase in the power density does not increase the gain coefficient, and (3) the C VI H_α line intensity from a capillary longer than 16 mm does not increase and tends to level off. It is suggested that there may be an optimum power density for a given capillary geometry, and that the capillary wall condition may be important, i.e., a newly drilled out capillary seems to be favored for the amplification. Surface condition effects have not been investigated so far.

IV. SUMMARY

The carbon plasma which is produced in a polyethylene capillary discharge is investigated using a two-meter grazing-incidence spectrograph monochromator. Space-resolved spectra are obtained using a toroidal mirror system and the electron temperatures are measured at both the axial and the peripheral region close to the capillary wall. There is a strong evidence of

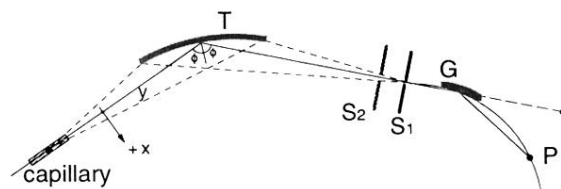
amplification at the cool ($T_e \sim 13$ eV) plasma region near the wall. Relative line intensities of the C VI H_α and a number of nongain lines are compared in this cool region as a function of capillary length. The C VI H_α line intensity increases exponentially whereas those of nongain transitions increase linearly with an increase of the capillary length. The gain coefficient thus measured indicates 2.8 cm^{-1} . The C VI H_α line intensity does not seem to increase exponentially beyond a capillary length of 16 mm and the gain-length product, gL , obtained here is 3.9, which is a typical value one would expect for a recombination soft-x-ray amplifier. The photoelectric signals of the C VI H_α line indicate that the amplification takes place about 40 ns after the current peak in the first half cycle of the capillary discharge, with a pulse width of 60 ns in FWHM. It is also important to note that there seems to be an optimum power input to the discharge for a given capillary geometry, and that the amplification lasts for only a few discharges with a freshly prepared capillary.

ACKNOWLEDGMENTS

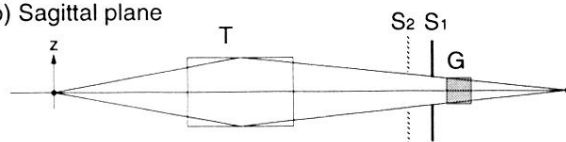
We would like to thank Dr. R. C. Elton for helpful comments. This research was partially supported by a POSCO basic research grant and also by the Korea Science and Engineering Foundation.

-
- [1] M. D. Rosen *et al.*, Phys. Rev. Lett. **54**, 106 (1985). D. L. Matthews *et al.*, *ibid.* **54**, 110 (1985).
 - [2] S. Suckewer *et al.*, Phys. Rev. Lett. **55**, 1753 (1985).
 - [3] C. H. Skinner, Phys. Fluids B **3**, 2420 (1991).
 - [4] A. Carillon *et al.*, Phys. Rev. Lett. **68**, 2917 (1992).
 - [5] S. Wang *et al.*, J. Opt. Soc. Am. B **9**, 360 (1992).
 - [6] B. J. MacGowan *et al.*, Phys. Fluids B **4**, 2326 (1992).
 - [7] J. A. Koch *et al.*, Phys. Rev. Lett. **68**, 3291 (1992).
 - [8] L. B. Da Silva *et al.*, Opt. Lett. **18**, 1174 (1993).
 - [9] Y. Nagata *et al.*, Phys. Rev. Lett. **71**, 3774 (1993).
 - [10] R. C. Elton, *X-ray Lasers* (Academic, San Diego, 1990).
 - [11] J. J. Rocca, D. C. Beethe, and M. C. Marconi, Opt. Lett. **13**, 565 (1988).
 - [12] C. Steden and H.-J. Kunze, Phys. Lett. A **151**, 534 (1990).
 - [13] J. J. Rocca, M. C. Marconi, and F. G. Tomasel, IEEE J. Quantum Electron. **29**, 182 (1993); C. A. Morgan, H. R. Griem, and R. C. Elton, Phys. Rev. E **49**, 2282 (1994).
 - [14] S. Glasstone and R. H. Lovberg, *Controlled Thermonuclear Reactions* (Van Nostrand, New York, 1960).
 - [15] T. N. Lee, Ann. N.Y. Acad. Sci. **25**, 112 (1975).
 - [16] P. Bogen, H. Conrads, G. Gatti, and W. Kohlhaas, J. Opt. Soc. Am. **58**, 203 (1968).
 - [17] R. A. McCorkle and H. J. Vollmer, Rev. Sci. Instrum. **48**, 1055 (1977).
 - [18] B. L. Henke *et al.*, J. Opt. Soc. Am. B **1**, 828 (1984).
 - [19] G. Tondello, Opt. Acta. **26**, 357 (1979).
 - [20] H. J. Shin *et al.* (unpublished).
 - [21] J. F. Seely, R. H. Dixon, and R. C. Elton, Phys. Rev. A **23**, 1437 (1981).
 - [22] G. J. Linford, E. R. Peressini, W. R. Sooy, and M. L. Spaeth, Appl. Opt. **13**, 379 (1974).
 - [23] R. W. Waynant and R. C. Elton, in *Organic Scintillators and Liquid Scintillation Counting* (Academic, New York, 1971), p. 467.

(a) Meridional plane



(b) Sagittal plane



T : toroidal mirror S1 : entrance slit (22 μm x 9 mm)
G : grating S2 : auxiliary slit (2 mm x 14 mm)
 $\phi \sim 85.7$ degree Sagittal focus at $\lambda = 28.7$ nm

FIG. 1. Schematic diagram showing the arrangement of the capillary light source, the toroidal mirror, and the grazing-incidence spectrograph: (a) view on the meridional (x,y) plane and (b) view on the sagittal (y,z) plane. Here, y axis indicates the optical axis defined by the spectrograph and the toroidal mirror system.

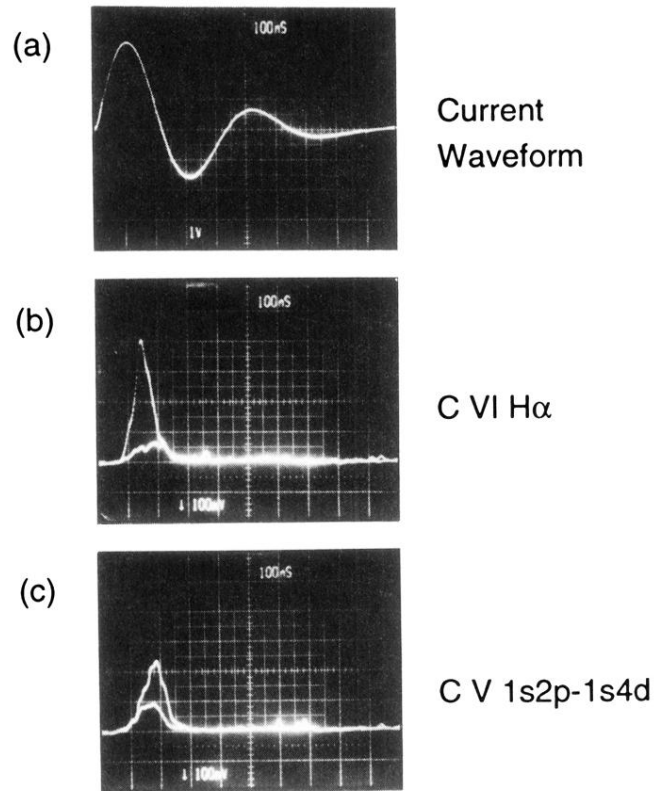


FIG. 8. Oscillograms of the discharge current wave form (a), the photoelectric signals of the amplified C VI H α line (b), and the C V 1s2p-1s4d line ($\lambda=18.67$ nm) (c). In (b) and (c), continuum signals near the respective line are superposed. In all cases, 14 mm long capillaries are used. Time scale is 100 nsec/div.